2-D Contact Detection and Localization Using Proprioceptive Information

Manfred Huber and Roderic A. Grupen

Laboratory for Perceptual Robotics
Department of Computer Science
University of Massachusetts

Technical Report #92-59
August, 1992

2-D Contact Detection and Localization Using Proprioceptive Information*

Manfred Huber and Roderic A. Grupen

Laboratory for Perceptual Robotics
Department of Computer Science
Lederle Graduate Research Center
University of Massachusetts
Amherst, Massachusetts 01003

submitted to the IEEE Transactions on Robotics and Automation as a REGULAR PAPER

Abstract

This paper employs proprioceptive information (joint angles and torques) to estimate properties of the contact between a planar robot and an unknown object without specifically requiring strategic manipulator motions. The algorithm presented tackles this task in two stages; a contact localization analysis is followed by a force domain contact detection analysis. In the former, the instantaneous center of velocity is used for each link to obtain an estimate of the location of a hypothetical contact point on the link surface. A second observer, based on the intersection of two consecutive postures of the manipulator provides an estimate of error associated with this location. Then this data is fused over time by tracking the contact location using a linear observer, resulting in a hypothesis for the location of a contact point under the assumption that a contact exists, an associated uncertainty region, and the surface normal for each link of the manipulator. The detection phase then uses torque domain evidence and the location estimates to verify the existence of each of the contacts. This process allows for the detection of multiple contacts on different links and provides estimates of contact location, velocity (rolling and sliding), surface normal, and contact force for each link.

1 Introduction

Perception of various aspects of the environment is essential for any agent to operate successfully in the real world. Each task requires thereby specific kinds of information and offers different means of obtaining it. In the case of manipulating objects, some of the most important information is the point of contact between an object in the environment and the manipulator and the Cartesian force resulting from their interaction. This data can then be used for such different actions as force control in a whole-arm manipulator [5], incremental grasp configuration in multifingered robot hands [6; 8] or modeling of unknown objects [1].

While vision could be used to obtain part of this information, it can not provide force data and has problems with concave objects and occlusions, illustrating the necessity of tactile sensing as a different sort of perception.

*This work was supported in part by NSF IRI-9116297 and CDA-8922572

When humans try to pick up an object in the dark, they first explore the location and shape of the object with the tactile sensors on their hand in order to determine the best grasp. To facilitate a similar performance for dextrous robot manipulators, anthropomorphic fingers with sensors [2] and tactile sensor arrays (see e.g. [11; 7] for an overview) have been developed and used for different tasks (e.g. [14; 3]). This approach, however, requires the distribution of many "taxels", and therefore wires and signal processing electronics, all over the manipulator leading to packaging problems and changes in the characteristics of the robot. This paper will therefore pursue a different path by using proprioceptive information.

In humans, the proprioceptive system provides internal information about stretch in the tendons, degree of muscle contraction and joint position which is used to determine the location of the limb (see e.g. [15] for details about human proprioception). Similar kinds of information are readily available for robot manipulators in the form of joint angles, velocities and torques.

Different methods to determine a contact point by means of this proprioceptive information have been proposed. While [5] shows a way to infer the location of the contact from the torques in two joints, [16] uses full force information (i.e. three forces and three moments) at the end of a probe for the same task in 3 dimensions. Since, however, all dynamic effects (and therefore movements) affect the output of the force/torque sensor, these techniques are very static. Because of this and the imprecise torque data obtained by current manipulators, the approach of [10; 9] first detects a contact by observing the torques and initiates then strategic posture changes while maintaining contact to determine the contact point and thus relies much less on the torque data. The role assignment to the different joints and the active movements, however, limit the detection to the most distal contact and doesn't allow for general movements. Another shortcoming is that a tactile sensor is assumed for the fingertip to detect any contacts occurring there. The algorithm presented in this paper tries to overcome these limitations for the planar case by employing the current motion of the finger. Three different observers based on geometric contact constraints and torque domain evidence are used to estimate the location and determine the existence of a contact for each link.

In the remainder of this paper, Section 2 introduces the constraints used in the algorithm while Section 3 discusses issues related to the modeling of uncertainties. Section 4 finally presents some results of this approach in a geometric modeling task.

2 Contact Constraints

The algorithm presented in this paper tries to use rigid body constraints and the violations of the equations of freespace dynamics to hypothesize the existence and location of contact points between a planar robot arm with revolute joints and parallel link surfaces and an unknown object. The object is assumed to be stationary and rigid and the robot provides the necessary information in the form of joint angles Θ_i, joint velocities $\dot{\Theta}_i$ and torques τ_i.

Figure 1 shows a three link manipulator of this type and some of the variables used throughout this paper, the most important of which are

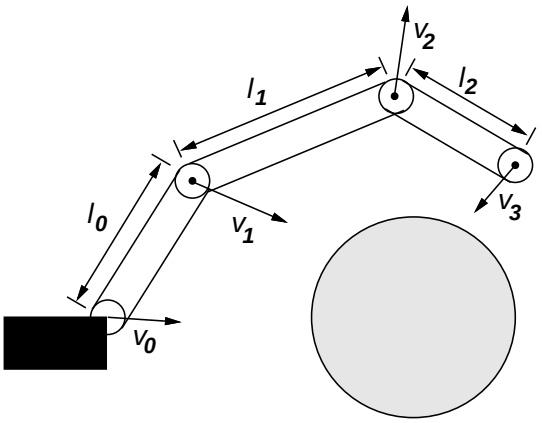

Figure 1: Planar Robot Arm with Spherical Object

Θ_i^t	Joint angle
$\dot{\Theta}_i^t$	Rotational velocity
τ_i^t	Joint torque
l_i	Link length
r_i	Half the width of the link
v_i^t	Cartesian velocity of joint axis
$p_i^t = \begin{pmatrix} x_i^t \\ y_i^t \end{pmatrix}$	Cartesian location of joint axis
P^t	Link Posture ,

where subscript i indicates the link/joint number and superscript t the time of the observation[1].

2.1 Link Contacts

Because of the differences in the surface geometry between the parallel link surfaces and the spherical tip and knuckle regions, these are treated separately. In this section the links are examined, where the location of a contact on link i is specified by the distance d_i^t from the proximal joint of this link and the side s of the link, which can be found based on the torques and is represented as 1 or -1 for the left or right side of the link, respectively (The computation of s is given by Equation 16).

2.1.1 Posture Intersection

Kaneko and Tanie [10] used the intersection of two consecutive postures as an approximation for the contact point. But while they used the intersection point for the link surfaces, this approach will employ a corrected form of the intersection for the link axis. Using the properties from Figure 3, equations for an intersection point ξ of the two link postures are given by

$$\xi = p_1^t + k^t \frac{1}{l} \begin{pmatrix} \ell_x^t \\ \ell_y^t \end{pmatrix}$$

[1] Subscripts and superscripts are avoided wherever possible to simplify the corresponding equations

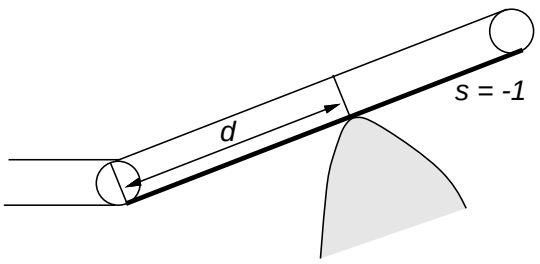

Figure 2: Internal Contact Coordinates

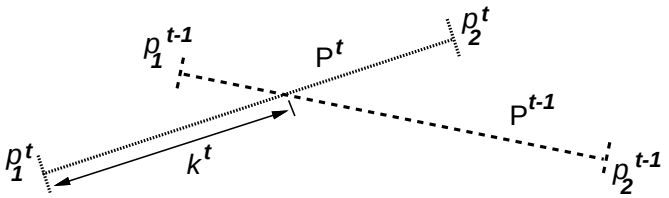

Figure 3: Postures at Time $t-1$ and t

$$(\xi - p_1^{t-1})^T \frac{1}{l} \begin{pmatrix} -\ell_y^{t-1} \\ \ell_x^{t-1} \end{pmatrix} = 0$$

where $\ell_x^t = x_2^t - x_1^t$.
From this, the intersection in internal coordinates can be derived as

$$k^t = l \frac{\Delta y_1 {\ell_x}^{t-1} - \Delta x_1 {\ell_y}^{t-1}}{{\ell_x}^t {\ell_y}^{t-1} - {\ell_y}^t {\ell_x}^{t-1}} \ . \tag{1}$$

This location k, however, is not the precise position of the contact point but only an approximation which depends on the curvature and the angle between the two postures. Therefore a compensation term is needed to shift this location to the real contact. In order to do this, the assumption is made, that the curvature of the object is constant between two consecutive posture recordings which leads to the picture shown in Figure 4 which also illustrates the properties used for the correction term. Using geometric properties for a link of width 0,

$$\begin{aligned} b &= r_o \varphi \\ y &= 2 r_o \sin \tfrac{\varphi}{2} \\ \delta_k &= \tfrac{y}{2} \tfrac{1}{\cos \frac{\varphi}{2}} \end{aligned}$$

the correction term δ_k can then be calculated as:

$$\delta_k = \frac{b}{\varphi} \tan \frac{\varphi}{2} \ ,$$

where b is the distance the contact point traveled on the object.

The introduction of a width for the finger changes y to $2(r_o + r) \sin \frac{\varphi}{2}$, which leads to

$$\delta_k = \left(\frac{b}{\varphi} + r \right) \tan \frac{\varphi}{2}. \tag{2}$$

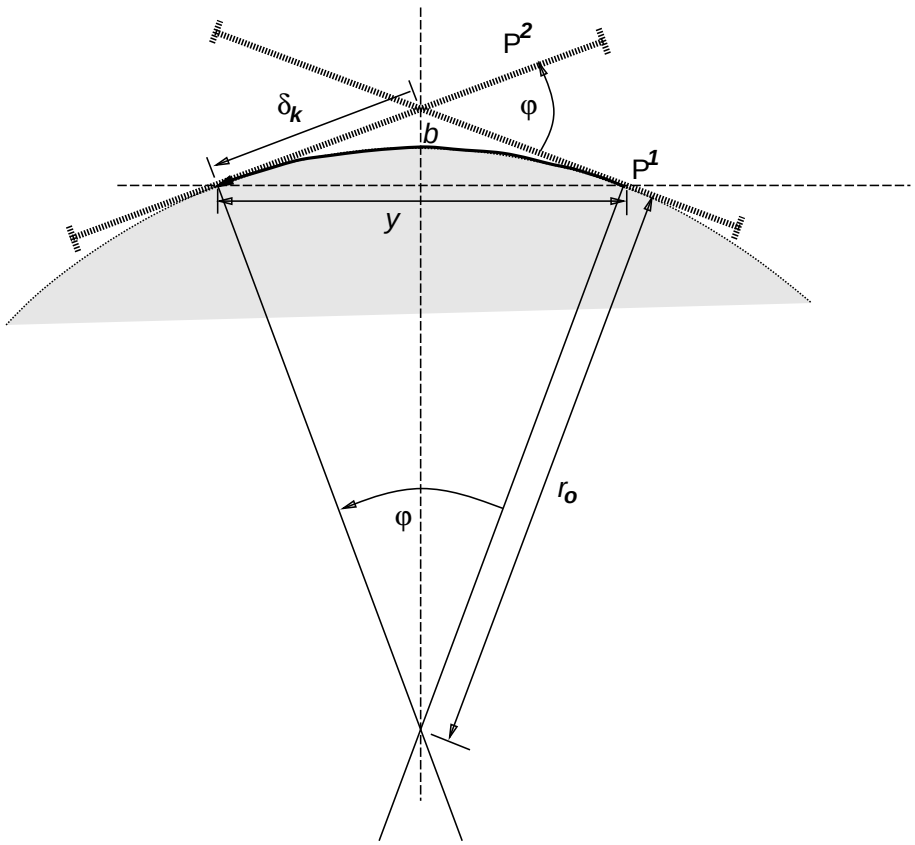

Figure 4: Correction of Intersection Point

Equations 1 and 2, finally, provide the corrected location of the contact $d^{'}$,

$$d^{'} = k + \delta_k \ . \tag{3}$$

The only unknown remaining is b, the distance the contact point traveled on the object which is equivalent to the distance it traveled on the link $d^t - d^{t-1}$ minus the distance the link slipped on the object.

2.1.2 Instantaneous Center of Velocity

Reuleaux [13] noted in 1875 that a lamina (or planar rigid body) moving continuously in the plane, can be shown equivalent to rolling a moving centroid over a fixed centroid. A direct consequence of this observation is that any planar motion of a lamina is equivalent to a pure rotation about an instantaneous center. The location of this point is the intersection of the two lines going through the two points p_i and p_{i+1} and orthogonal to the corresponding velocity vectors. This construction using the endpoints of link i is shown in Figure 5.

In the case of a contact without slip between this link and a rigid object, this center would be on the surface of the link because it rotates instantaneously around the contact point. In most situations, however, the link will slip at least slightly over the contact point which means that the instant center moves away from the link surface. Therefore the slip velocity, which is always tangential to the link surface, has to be compensated for in order to find the point of contact.

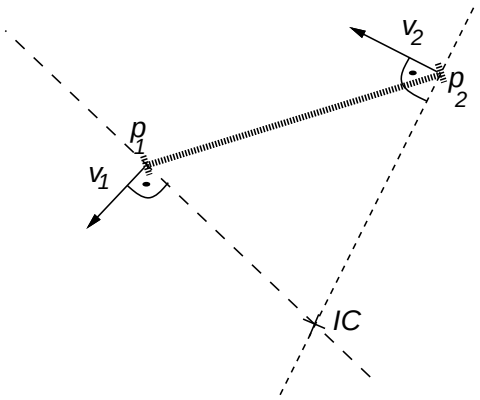

Figure 5: Instant Center for one Link

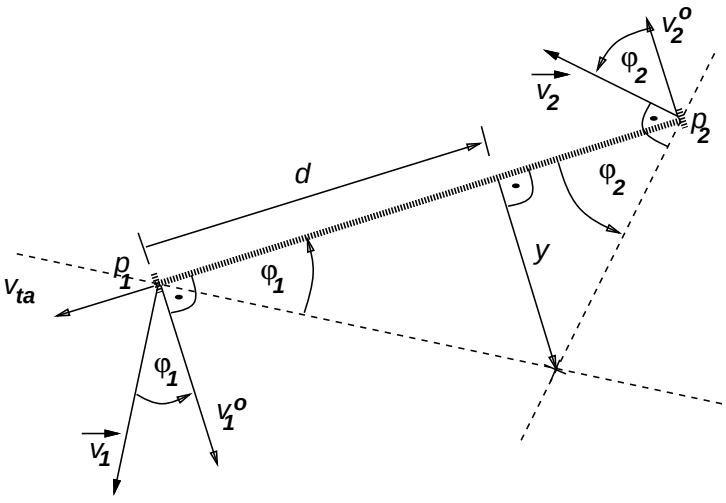

Figure 6: Instant Center for Contact with Slip

In the following analysis, $\hat{\ell}$ denotes the unit vector along the link and $\hat{n}$ is orthogonal to the link axis.

$$\hat{\ell} = \frac{1}{l}\begin{pmatrix} \ell_x \\ \ell_y \end{pmatrix} = \frac{1}{l}(p_2 - p_1)$$
$$\hat{n} = \frac{1}{l}\begin{pmatrix} -\ell_y \\ \ell_x \end{pmatrix} .$$

The orthogonal and tangential components of the link endpoint velocities, v_i^o and v_{ta}, are therefore found as $v_i^o = \hat{n}^T v_i$ and $v_{ta} = \hat{\ell}^T v_1$, respectively and together with the geometric properties shown in Figure 6, the following system of equations can be derived

$$\begin{aligned} \tan(\varphi_1) &= \tfrac{v_{ta}}{v_1^o} \\ \tan(\varphi_2) &= -\tfrac{v_{ta}}{v_2^o} \\ \tan(\varphi_1) &= -\tfrac{y}{d} \\ \tan(\varphi_2) &= -\tfrac{y}{l-d} \ , \end{aligned}$$

which result in an expression for the location of the instantaneous center.

$$\begin{aligned} d &= l\tfrac{v_1^o}{v_1^o - v_2^o} \\ y &= l\tfrac{v_{ta}}{v_2^o - v_1^o} \end{aligned} \tag{4}$$

This means that in the presence of a contact, besides establishing the location d of the contact point, the position of the center also determines the slip velocity if the joint velocities and width of the finger are known because for link i, $v_2^o - v_1^o = l\sum_{j=0}^{i}\dot{\Theta}_j$.

2.2 Tip Contacts

As in the case of the link, a relation between the motion and the contact point exists also for the spherical tip and knuckle regions. In the following this relation will be used to find the contact location represented as the angle ϕ towards the surface normal of the object.

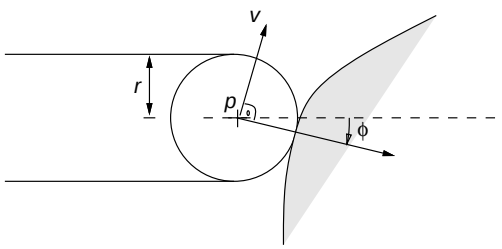

Figure 7: Tip Contact Representation

2.2.1 Velocity-Location Relation

In the presence of a tip contact, all the Cartesian velocity is tangential to the surface of the object at the point of contact. As shown in Figure 7, the direction of the surface normal, and with it the contact location ϕ, is therefore perpendicular to the endpoint velocity

$$\begin{pmatrix} \cos\phi \\ \sin\phi \end{pmatrix} = \pm\frac{1}{\|v\|}\begin{pmatrix} -v_y \\ v_x \end{pmatrix} , \tag{5}$$

which leaves two possible points for a full sphere but since the tip is only a hemisphere, only one of the solutions remains.

2.2.2 Displacement-Location Relation

In the same way as the endpoint velocity, the displacement $\Delta p = \begin{pmatrix} \Delta x \\ \Delta y \end{pmatrix}$ for two consecutive postures can be used to get an estimate ψ of the contact location, where

$$\begin{pmatrix} \cos\psi \\ \sin\psi \end{pmatrix} = \pm \frac{1}{\|\Delta p\|} \begin{pmatrix} -\Delta y \\ \Delta x \end{pmatrix} . \tag{6}$$

This position, however, is only an approximation which depends on the curvature of the object and therefore a correction term is needed to obtain the precise location. Figure 8 shows this and the geometric terms used to obtain the correction δ_ψ under the assumption that the curvature of the object is constant between the two posture recordings.

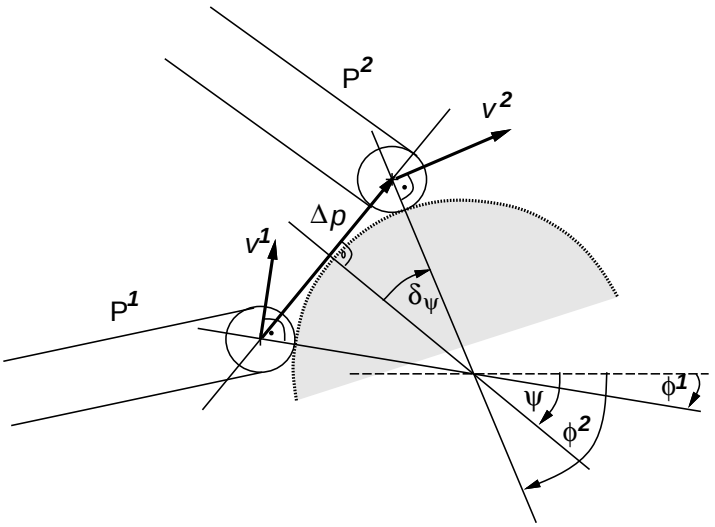

Figure 8: Correction for Displacement Based Point

Because of the constant curvature, the correction term can be found as

$$\delta_\psi = \frac{1}{2}\left(\phi^2 - \phi^1\right) \tag{7}$$

and therefore the corrected angular representation of the contact is

$$\phi' = \psi + \delta_\psi \ . \tag{8}$$

3 The Algorithm

Geometric relations like those described in the previous section, only yield exact results if all the variables are precisely known. In a robot environment, however, sensor readings are imprecise, objects are not perfectly rigid and other kinds of noise exist. Therefore a way has to be found to incorporate these uncertainties. The algorithm presented in this section tries to cope with these problems by means of filtering and worst case analysis.

After transforming the angular data into Cartesian coordinates, the algorithm works in the following three stages:

1. Possible contact positions and normals for each link are estimated by means of position and velocity evidence, based on the assumption that contact exists.
2. Constraints on the position and velocity of contact points are used to decide whether a link or tip contact is more probable.
3. Torque evidence is utilized to verify the existence of a contact point and to estimate the corresponding contact force.

3.1 Contact Localization

In the localization step, the fact that a contact point generally moves continuously over the surface of the link, allows to use a filter to include inaccuracies of the locations given by the geometric considerations of Section 2. All links are thereby strictly independent i.e. that no results from one link influence any other link.

3.1.1 Link Contacts

Because of the known kinematics of the manipulator, Equation 4 provides an estimate of the slip velocity of the link on the object and a hypothesis of the contact location. In order to obtain a better estimate, the contact point is tracked along the link, including the new hypothesis using a linear observer. This allows the combination of old and new evidence to a more precise location $\hat{d}$ and a qualitative estimate of the uncertainty for this location.

The means of doing this integration is a linear Kalman filter (see e.g. [4]) using the system description

$$\begin{aligned} \bar{d}^t &= \bar{d}^{t-1} + v_c \Delta t + \varrho^{t-1} && \text{as a system model} \\ d &= d_c + \rho^{t-1} && \text{for the new measurement} \end{aligned}$$

where,

$$\begin{aligned} \bar{d}^t &= \text{Contact location at time } t \\ \varrho^t &= \text{Noise process described by } N\left(0, \sigma_\varrho^2(t)\right) \\ d_c &= \text{Actual contact position} \\ \rho^t &= \text{Noise process described by } N\left(0, \sigma_\rho^2(t)\right) . \end{aligned}$$

Since the variances $\sigma_\varrho^2(t)$ and $\sigma_\rho^2(t)$ are not known they are replaced by error estimates $\varepsilon_{v_c}\Delta t$ and ε_d for the prediction and measurement, respectively. Using this and an a priori knowledge of the situation at time $t-1$, the estimator equations are:

$$\begin{aligned} \hat{d}^t &= \left(\hat{d}^{t-1} + v_c \Delta t\right) + \frac{\hat{\varepsilon}^{t-1} + \varepsilon_{v_c}\Delta t}{\varepsilon_d + \hat{\varepsilon}^{t-1} + \varepsilon_{v_c}\Delta t}\left(d - \left(\hat{d}^{t-1} + v_c \Delta t\right)\right) \\ \hat{\varepsilon}^t &= \frac{\varepsilon_d\left(\hat{\varepsilon}^{t-1} + \varepsilon_{v_c}\Delta t\right)}{\varepsilon_d + \hat{\varepsilon}^{t-1} + \varepsilon_{v_c}\Delta t} , \end{aligned} \tag{9}$$

with,

$$\begin{aligned} \hat{d}^t &= \text{Filtered location at time } t \\ d &= \text{Location hypothesis of Equation 4} \\ v_c &= \text{Contact point velocity on the link} \\ \hat{\varepsilon}^t &= \text{Uncertainty associated with } \hat{d}^t \\ \varepsilon_d &= \text{Uncertainty associated with } d \\ \varepsilon_{v_c} &= \text{Uncertainty associated with } v_c . \end{aligned}$$

In order to use this observer, however, values for the unknown variables v_c, ε_{v_c} and ε_d have to be found. For the former two, a filtered version of $\frac{\Delta \hat{d}}{\Delta t}$ and $\frac{\hat{\varepsilon}^t + \hat{\varepsilon}^{t-1}}{\Delta t}$ can be used as an approximation of the actual contact velocity on the link and the corresponding uncertainty. The derivation of an estimate for the latter, using the intersection hypothesis $d^{'}$ as a second observer, is shown in the next section.

3.1.2 Uncertainty Propagation for Link Contacts

If the object is rigid, its curvature is constant between two posture recordings and that the link contacts the object in both postures, the intersection point k of the two snapshots can be computed correctly. The second value needed to calculate $d^{'}$ is the correction term of Equation 2. This term, however, contains, besides the angular displacement $\varphi = \sum \Delta\Theta_j$, the distance b that the contact traveled on the object surface. An estimate for this term can be found from the relation

$$(b + d_s) \cong \left(d - \hat{d}^{t-1}\right) \ ,$$

where, assuming a constant slip acceleration between two observations.

b	= Distance due to rolling
$d_s = \frac{v_s^t + v_s^{t-1}}{2}\Delta t$	= Distance due to slip
v_s^t	= Slip velocity derived from Equation 4
d	= Current instant center observation
$\hat{d}^{t-1}$	= Last estimate

Taking this estimate for b, an intersection hypothesis $d^{'}$ can be derived as a second observation, based on the correctness of the variables used. In reality, however, the current observation and the previous estimate may both have associated errors in the range of $\pm\varepsilon_d$ and $\pm\hat{\varepsilon}^{t-1}$, respectively. Since an error estimate for the previous estimate is given a priori by the filter in Equation 9 , the worst case error in the new observation can be found using Equations 2 and 3 by assuming that the actual ocation of the contact $d_c = d \pm \varepsilon_d$. Using this leads to

$$d_c - k = \left(\frac{d \pm \varepsilon_d - \hat{d}^{t-1} \pm \hat{\varepsilon}^{t-1} - d_s}{\varphi} + r\right) \tan\frac{\varphi}{2} \ ,$$

which can be transformed into

$$\pm\varepsilon_d = \frac{\pm\hat{\varepsilon}^{t-1}\frac{1}{\varphi}\tan\frac{\varphi}{2} + d^{'} - d}{1 - \frac{1}{\varphi}\tan\frac{\varphi}{2}}$$

and results in an expression for the error bound in the contact location estimate,

$$\varepsilon_d \leq \frac{\hat{\varepsilon}^{t-1}\frac{1}{\varphi}\tan\frac{\varphi}{2} + \left|d^{'} - d\right|}{1 - \frac{1}{\varphi}\tan\frac{\varphi}{2}} \qquad \text{for } \frac{\tan\frac{\varphi}{2}}{\varphi} < 1 \ . \tag{10}$$

This term can now be used in Equation 9 to compute the contact location.

A second possible choice for ε_d would be a heuristic based on Equation 10 and other evidence such as the difference between the new observation d and the predicted location $\hat{d}^{t-1} + v_c\Delta t$, the advantage of such a heuristic being that it could be a much less conservative estimate than the one represented by Equation 10 alone and therefore lead to tighter error bounds for the points.

3.1.3 Tip Contacts

Similar to the case of the link, the behavior of a tip contact can be expressed using the linear equations

$$\begin{aligned} \bar{\phi}^t &= \bar{\phi}^{t-1} + \omega \Delta t + \varrho^{t-1} && \text{for the system} \\ \phi &= \phi_c + \rho^{t-1} && \text{as a measurement model} \end{aligned}$$

with

$$\begin{aligned} \bar{\phi}^t &= \text{Contact location at time } t \\ \varrho^t &= \text{Noise process described by } N\left(0, \sigma_\varrho^2(t)\right) \\ \phi_c &= \text{Actual contact position} \\ \rho^t &= \text{Noise process described by } N\left(0, \sigma_\rho^2(t)\right) . \end{aligned}$$

Replacing the variances again with error estimates results in a location estimate $\hat{\phi}$ and an estimate of the corresponding angular uncertainty. The equations for this filter are nearly identical to those used for the link.

$$\begin{aligned} \hat{\phi}^t &= \left(\hat{\phi}^{t-1} + \omega \Delta t\right) + \frac{\hat{\epsilon}^{t-1} + \epsilon_\omega \Delta t}{\epsilon_\phi + \hat{\epsilon}^{t-1} + \epsilon_\omega \Delta t} \left(\phi - \left(\hat{\phi}^{t-1} + \omega \Delta t\right)\right) \\ \hat{\epsilon}^t &= \frac{\epsilon_\phi \left(\hat{\epsilon}^{t-1} + \epsilon_\omega \Delta t\right)}{\epsilon_\phi + \hat{\epsilon}^{t-1} + \epsilon_\omega \Delta t} , \end{aligned} \tag{11}$$

where,

$$\begin{aligned} \hat{\phi}^t &= \text{Filtered location at time } t \\ \phi &= \text{Location hypothesis of Equation 5} \\ \omega &= \text{Angular contact point velocity} \\ \hat{\epsilon}^t &= \text{Uncertainty associated with } \hat{\phi}^t \\ \epsilon_\phi &= \text{Uncertainty associated with } \phi \\ \epsilon_\omega &= \text{Uncertainty associated with } \omega \end{aligned}$$

The variables ω and ϵ_ω are similarly given by $\frac{\Delta \hat{\phi}}{\Delta t}$ and $\frac{\hat{\epsilon}^t + \hat{\epsilon}^{t-1}}{\Delta t}$. To determine the remaining unknown ϵ_ϕ, the displacement based hypothesis ϕ' of Equation 8 is employed, using ϕ and $\hat{\phi}^{t-1}$ as the contact locations for the two postures. As in the case of the link, this leads to an error analysis using Equation 7 and 8 described in the next section.

3.1.4 Uncertainty Propagation for Tip Contacts

Making the same assumptions as in the case of the link contacts, and setting the correct contact location to $\phi_c = \phi \pm \epsilon_\phi$ yields

$$\phi_c - \psi = \frac{1}{2}\left(\phi \pm \epsilon_\phi - \hat{\phi}^{t-1} \pm \hat{\epsilon}^{t-1}\right) ,$$

which leads to

$$\pm \epsilon_\phi = \pm \hat{\epsilon}^{t-1} + 2\left(\phi' - \phi\right)$$

and finally provides a worst case error which can be used directly or as part of a heuristic in the filter of Equation 11.

$$\epsilon_\phi \leq \hat{\epsilon}^{t-1} + 2\left|\phi' - \phi\right| \tag{12}$$

3.2 Link/Tip Decision

Since tip and link are treated separately in the contact localization phase, it results in a possible contact location for the link and one for the tip which are both maximally consistent with the corresponding constraints. In most cases, however, only one of the two contact points with the object exists. It is therefore necessary to decide which of the two estimates is the correct one. In order to do this, additional constraints on the location and the motion of the contact point are used as counterevidence for the existence of one of the two alternatives[2].

3.2.1 Impossible Location of Link Contact

The first and most obvious evidence against the existence of a link contact is found in the location of the estimate. Since this location is based on the instantaneous center of rotation, many situations with a tip contact result in a hypothesis outside the actual link surface (i.e. $\hat{d} < 0 \ \vee \ \hat{d} > l$). Taking the uncertainty associated with the location into consideration, this can be formed into a measure of evidence $E^-_{\hat{d}}$ against a link contact, where

$$E^-_{\hat{d}} = \begin{cases} \frac{\hat{d}-l}{\hat{\varepsilon}} & \text{for } \hat{d} > l \\ \frac{-\hat{d}}{\hat{\varepsilon}} & \text{for } \hat{d} < 0 \\ 0 & \text{otherwise .} \end{cases} \tag{13}$$

3.2.2 Impossible Motion of Link Contact

A second constraint for the link contact concerns its motion. In the absence of slip, the orientation of the rotation of the link around the contact point determines whether the contact moves up or down this link as shown in Figure 9.

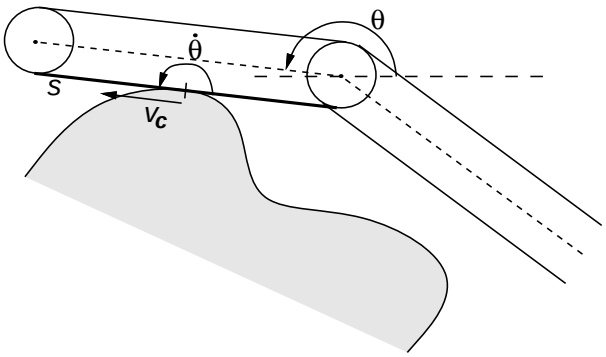

Figure 9: Contact Point Velocity without Slip

Including slip and relating this to the uncertainty involved in the contact velocity results in a second counterevidence measure $E^-_{v_c}$ with

$$E^-_{v_c} = \frac{\max\left(0, \ -s \cdot sign\left(\dot{\theta}\right)\left(v_c - v_s\right)\right)}{\varepsilon_{v_c}} , \tag{14}$$

where

[2]It has to be mentioned here, that this can not succeed in general because of the possibility of having simultaneous contacts on concave objects. The motions in these cases can produce the same sensory signature as either of the equivalent single contact cases leading necessarily to a wrong decision

v_c = Contact velocity used in Equation 9
v_s = Slip velocity determined by Equation 4
s = Contact side of the link
$\dot{\theta}_i = \left(\sum_{j=0}^{i} \dot{\Theta}_j\right)$ = Rotational velocity of link i .

3.2.3 Impossible Location of Tip Contact

In a similar way, a restriction for the location of possible tip contacts exists. Since the side s for the link position is based on torque evidence and thereby on the contact force, it also applies to the tip and indicates on which side of the link axis the contact has to be. Using this, the location $\hat{\phi}$ of the contact can be tested and evidence $E_{\hat{\phi}}^{-}$, this time against the existence of the hypothesized tip contact, can be found as

$$E_{\hat{\phi}}^{-} = \frac{\max\left(0,\ -s\left(\hat{\phi} - \theta\right)\right)}{\hat{\epsilon}} \ , \tag{15}$$

where

$\theta_i = \sum_{j=0}^{i} \Theta$ = Angular orientation of link i
$\left(\hat{\phi} - \theta\right)$ scaled between $-\pi$ and π .

These three sources of evidence, quantified by Equations 13, 14 and 15 can then be combined in a heuristic to form the decision for either the link or tip contact, resulting in a single contact hypothesis per link [3].

3.3 Contact Detection

While all the kinematic constraints used so far give a hypothesis about the possible location of a contact, they can not determine the existence of it. The reason for this lies within the fact that the criteria in the localization stage are purely based on the motion of the finger which can always be 'simulated' in the absence of an interaction with the environment. Therefore other sources of information have to be used in order to decide this question. One possibility is to use the joint torques τ as a third 'observer' to verify the existence of a contact and to provide information about the side s used in the previous sections for the localization of link contacts.

3.3.1 Torque Decomposition

Since each interaction between an object and the manipulator results in a force producing torques in the joints, each contact with an object leads to a violation of the equations of freespace dynamics of the robot. A single contact produces thereby a unique set of joint torques but since it causes torques in all proximal joints, this torque information gets ambiguous in the presence of multiple contact points. Under the assumption that the location and surface normal for the most

[3] The term used for the experiments in Section 4, for example, is the simple linear combination

$$sign\left(0.5 + E_{\hat{\phi}}^{-} - E_{\hat{d}}^{-} - E_{v_c}^{-}\right) \ , \text{ where 1 denotes link and } -1 \text{ tip contact.}$$

distal contact are known and that no friction and dynamic effects are present, however, the acting contact force and thereby the existence of this contact can be determined by analyzing only the torque of the proximal joint of the corresponding link. In this case, the side information s can be simply found as

$$s = sign(\tau) \tag{16}$$

because of the relation between the contact force and the torque in this joint. For the derivation of the magnitude of the force for a frictionless contact, some additional considerations are necessary as illustrated in Figure 10, which also shows the variables used.

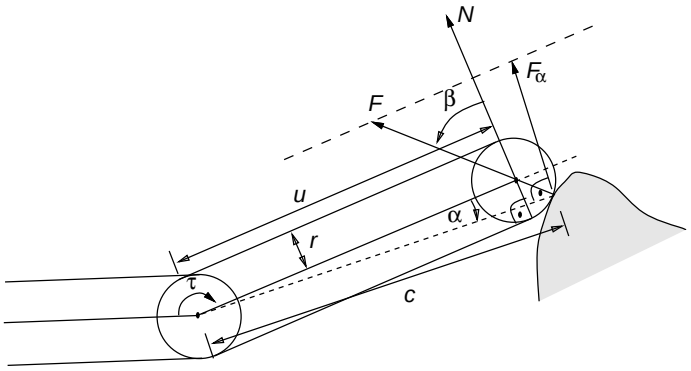

Figure 10: Contact Force Construction

From this construction, relations between the different properties arise as

$$\begin{array}{rl} c & = \sqrt{(u + r\sin\beta)^2 + (r\cos\beta)^2} \\ \begin{pmatrix} \sin\alpha \\ \cos\alpha \end{pmatrix} & = \frac{1}{c}\begin{pmatrix} r\cos\beta \\ u + r\sin\beta \end{pmatrix} \\ |F_\alpha| & = \frac{|\tau|}{c} \end{array}$$

and the contact force F is therefore given by

$$|F| = \frac{|F_\alpha|}{\cos(\alpha+\beta)} = \frac{|\tau|}{c \cdot \cos(\alpha+\beta)} \tag{17}$$

for a point contact without friction[4], where

$$\left.\begin{array}{ll} u & = \hat{d} \\ \beta & = (s+1)\frac{\pi}{2} \end{array}\right\} \text{ for link contacts}$$

$$\left.\begin{array}{ll} u & = l \\ \beta & = \frac{\pi}{2} + \hat{\phi} - \sum_{j=0}^{i}\Theta_j \end{array}\right\} \text{ for tip contacts .}$$

This calculation is possible because the direction of the force coincides with the surface normal of the link at the contact point (which is identical to the surface normal of the link at this location) and allows to calculate the torques produced by this contact force in all the proximal joints of the corresponding link i via the relation

$$\vec{\tau} = J_i^T F \tag{18}$$

[4]This equation could be simplified to $F = \frac{|\tau|}{u\cos\beta}$, which can also be derived in a much easier way. This simpler formulation, however, does not allow for an easy incorporation of Coulomb friction.

where J_i is a partial Jacobian of the manipulator using $l_i = c$, $\Theta_i = \Theta_i + \alpha$ and $l_j = 0$ for $j > i$.

Subtracting these resulting torques from the measured ones leaves only the torques caused by more proximal contacts and thus the same can be done for the next link, allowing to decompose the torque information into the components due to individual contact points and to decide their existence.

3.3.2 Incorporation of Uncertainties

Movements of the manipulator always cause dynamic torques and thus not all the measured torque is really due to the contact. To be able to do the decomposition under these circumstances it is therefore necessary to compensate for the dynamics of the robot which means that a model of the freespace dynamics has to be available. Since this model is in most cases not perfect, the minimum and maximum values are used here in order to make a worst case analysis of the torque data [5].

In the same way as the extreme cases of the manipulator dynamics, the uncertainties in the location of the link contact $\pm\hat{\varepsilon}$ and in the direction of the force $\pm\hat{e}$ for tip contacts allow for variations in the contact force and thereby in the resulting torques. In order to decide the existence of a contact it is therefore necessary to find out if the measured torque is outside the resulting 'torque interval' created by all the uncertainties. Thus the extreme torque values due to the dynamics and distal contacts have to be calculated for all the joints. Because the function for torques in the proximal joints is monotonic in the location u and the angle β [6], it is sufficient to calculate the torques due to the present contact for all combinations of the extreme location values u and β using Equations 17 and 18 and use the extrema of the resulting torque for each joint to determine the existence of a contact.

Using this approach, all the location uncertainties of the previous sections can be integrated, allowing for a decision based on the whole uncertainty intervals for each contact point and the dynamics of the robot. As a result of this exponential process, possible ranges of contact forces can be associated with each contact point which could be used e.g. for control purposes.

3.3.3 Friction

All the considerations so far have been based on the assumption of the absence of friction, which is not realistic. Therefore a way to incorporate it into the algorithm is shown in this section using Coulomb friction as a model.

Coulomb friction can be seen as a pure uncertainty in the direction of the contact force, represented by the friction cone (or half the cone if the direction of slip is known) and does therefore not interfere in any way with the kinematic constraints used in the localization stage. The only changes are thus necessary in the detection phase. There the uncertainty in the direction of the force has to be integrated in the calculation of the contact forces and thus of the worst case torques. This, however, can easily be done by adapting Equation 17 to

$$|F| = \frac{|\tau|}{c \cdot \cos(\alpha + \beta \pm \vartheta)} , \tag{19}$$

where,

$$\tan\vartheta = \mu_f = \text{maximum coefficient of friction}$$
$$(\alpha + \beta + \gamma) \in \left((2k-1)\tfrac{\pi}{2}, (2k+1)\tfrac{\pi}{2} \right) .$$

[5] It has to be noted here that an accurate model is not required in most cases since the contact localization can be expected to occur during low velocity movements and therefore only needs good inertial parameters.

[6] A proof for this is given in the Appendix

Using this in the calculations of Section 3.3.2 provides a worst case analysis that includes Coulomb friction.

4 Experiments

4.1 Simulation Results

The performance results presented in this section were obtained from a dynamic robot simulator, modeling the object surface as a damped spring. The objects are therefore not perfectly rigid and introduce uncertainty into the analysis. For the algorithm, the pure worst case error estimates of Equations 10 and 12 are used in the filters of Equation 9 and 11, respectively, and the simple heuristic, $sign(0.5 + E^-_{\hat{\phi}} - E^-_{\hat{d}} - E^-_{v_c})$, with 1 denoting link and -1 tip contact is employed for the link/tip decision process. The "finger" links are $0.22225m$, $0.15875m$, and $0.127m$ in length respectively from the finger's coordinate frame. Compliant motion of the finger is generated by a PD controller, regulating the finger's position relative to reference angles $\Theta_{ref_i} = \pi/4$. The finger's coordinate frame is then displaced with a constant speed ($0.33m/s$) in the negative x-direction. To illustrate the performance of the algorithm, both smoothly curved and polygonal objects are presented and the data is discussed.

Figure 11 shows a sequence of snapshots of the robot interacting with a circular object and the data obtained during this movement. The radii of the circles representing the contact estimates denote the associated uncertainty obtained by the Kalman filter of the localization part. The statistics on the right show probability distributions for the absolute distance between the object surface and the hypothesized contact points.

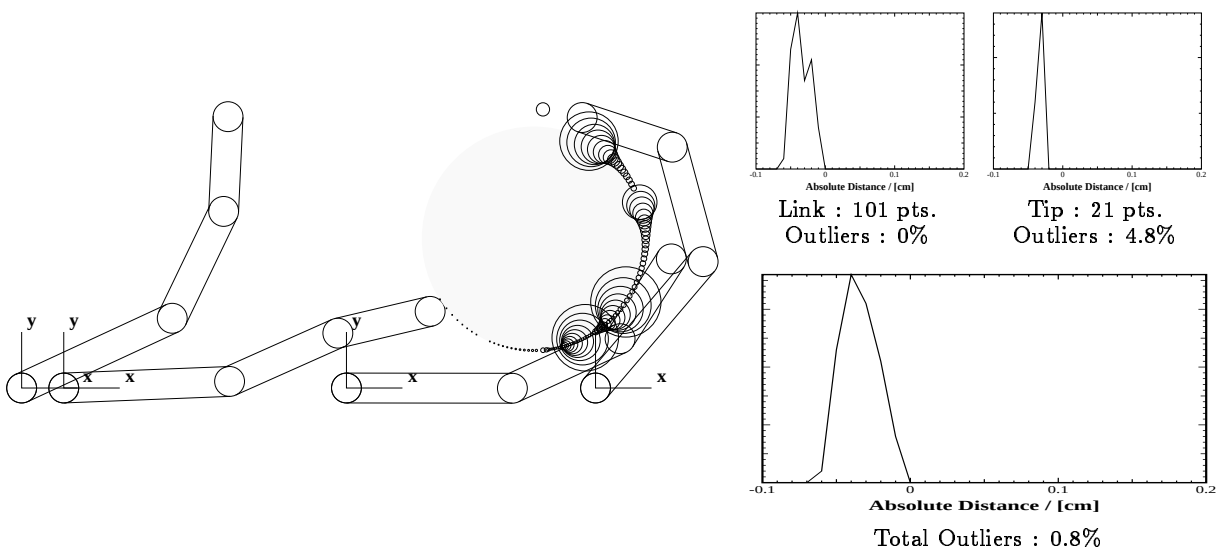

Figure 11: Absolute Distance Error for Spherical Object

This data shows only one tip contact point outside the object while all the other estimates are up to $0.6mm$ inside the object (recall that this is an elastic object and that the manipulator must push on it to observe it). The obvious outlier directly above the object is due to a incorrect decision for the tip instead of the link during the initial contact.

A convex polygon as a second object is presented in Figure 12.

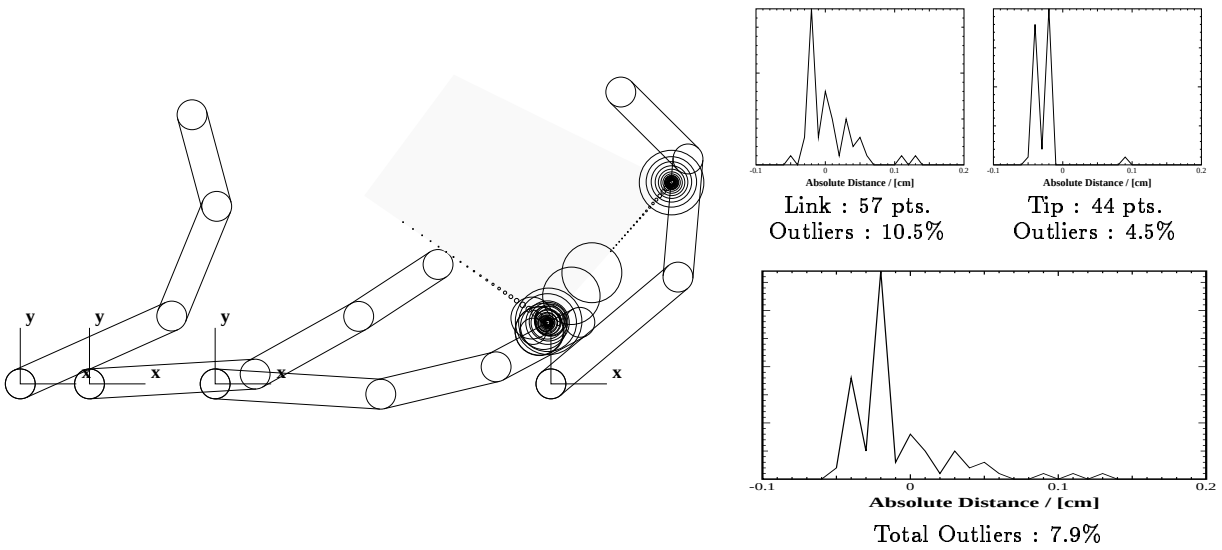

Figure 12: Absolute Distance Error for Convex Object

For this object, 7.9% of the points are more than $2mm$ outside the object. This much higher error is mainly due to link contacts because of the sudden changes from tip to link contacts which means that the contact point is not moving continuously over the arm surface and therefore not all the assumptions are fulfilled. Looking at the ratio between the absolute distance and the error estimate, however, shows that for only 1.8% of the link contacts the estimate is too small and for 96% of all points the true location is within the uncertainty interval.

As a last object, Figure 13 shows this movement and the results for a concave polygon.

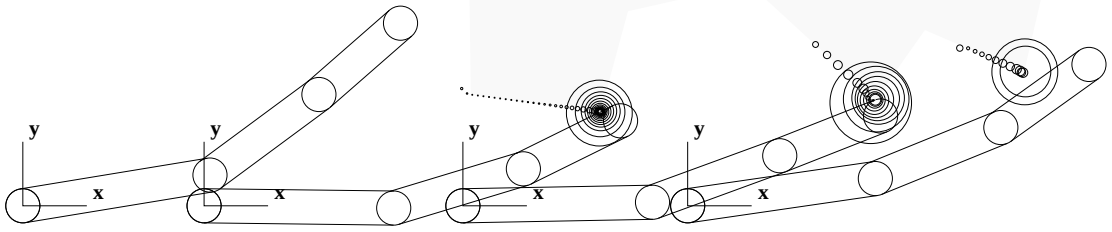

Figure 13: Contacts for Concave Object

Some of additional problems arising with this object are the sudden switches from one contact location to an different one or the existence of multiple contacts on one link and the fact that the loss of contact at the concavities introduces additional dynamic effects in the manipulator. One of the effects of discontinuities in the surface curvature can be seen here in the 'overshoot' at the lower left corner. The reason for this is that because of the consistency of the previous estimates,

while sliding along the face of the polygon, decreases the influence of the new measurement on the new estimate, resulting in only slow adaptation to the new surface orientation. In general, worse results can be expected in this case. Figure 14 shows statistics of the absolute error and the one related to the error estimate for this object.

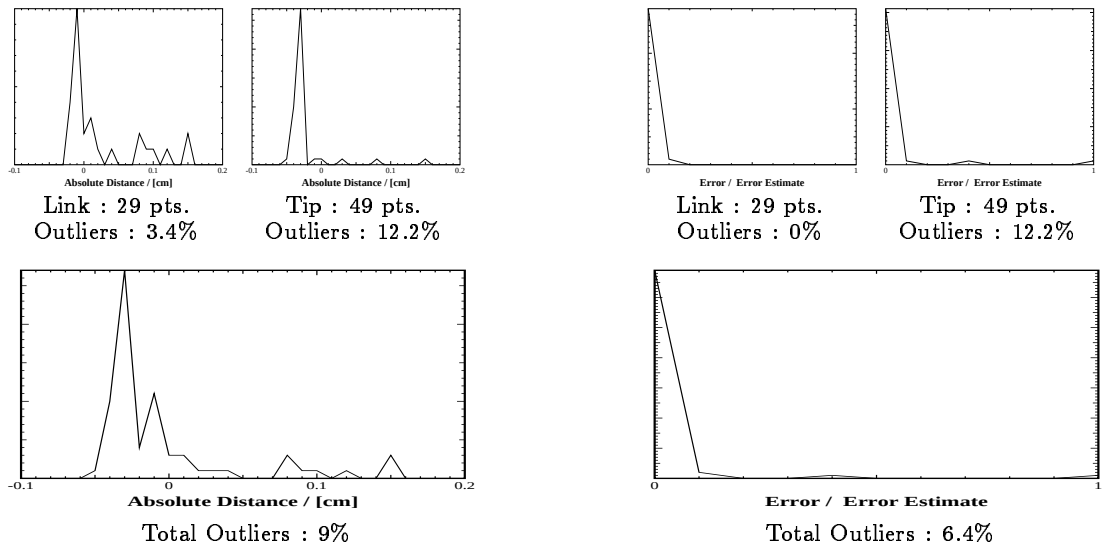

Figure 14: Absolute and Relative Distance Error for Concave Object

As expected, a higher number of outliers can be found here, leaving still 91% of all points within the range of $2mm$ and 93.6% within their associated error estimates.

These results show that the approach presented here expands to different object shapes although they don't fulfill all the assumptions used for the geometric analysis. Moreover, these examples violate the rigid body assumption and do not maintain contact continuously during the interaction. These examples illustrate that the algorithm can successfully cope with these inconsistencies in some cases.

5 Conclusions

The algorithm presented in this paper permits the gathering of contact information while interacting with an unknown object using only joint angle and torque sensors without restricting the movements and therefore not interfering with other robot behaviors. Although the analysis is based on rigid objects and some additional assumptions, the experiments performed show that this approach is also able to handle objects which don't fulfill all these requirements.

For tasks like geometric modeling, where gathering information is the main objective, it is possible that the quality of the data can be improved by executing specific movements to verify previous contact estimates and follow the contours of the object. Such an active sensing strategy may not always be possible in general due to constraints imposed by other objectives in the manipulation task. For this reason, we felt it was important to develop a sensing algorithm which could gather information opportunistically during general interactions with the object.

Implementations of this algorithm on real robots requires some of the equations to be changes to reflect the actual arm geometry. The influence of such a change, however, is limited to changes in the equations of Section 2 for the intersection and instantaneous center, but the underlying algorithm

is unchanged. Future extensions of this work will consider more general geometric representations for the manipulator which may alleviate re-deriving this relations for each manipulator. Moreover, some of the problems encountered because of the non-uniform treatment of the link and the tip may also be removed.

When cast into three dimensions, the intersection and instant center hypothesis each result in a curve rather than a point on the link surface. A measurement of the location of a contact point can therefore be found by intersecting these two curves with an associated uncertainty based on a term derived from an error analysis similar to the one of Section 3.1.2 and the angle between the tangents of the curves at the hypothetical location. Once again, the Kalman filter can be used for fusion over time, in this case, however, the filter produces an estimate of a two parameter contact location. Moreover, in addition to verifying already localized contacts, torque information can be used to hypothesize the contact location itself, since the localization uncertainty can be resolved to some degree by the three dimensional line of force generated by the manipulator along the link in question.

A. Appendix

Assuming a contact on link n at distance c with an angle towards the link normal of γ, the torque τ_m at link m caused by this contact is

$$\tau_m = |F|\, J_n^T \begin{pmatrix} -\sin\left(\sum_{j=0}^{n} \Theta_j + \gamma\right) \\ \cos\left(\sum_{j=0}^{n} \Theta_j + \gamma\right) \end{pmatrix} .$$

Using Equation 17 and the Jacobian leads than to

$$\tau_m = \frac{|\tau_n|}{c\cos\gamma} \sum_{j=m}^{n-1} \left(\left(l_j \sin \sum_{k=0}^{j} \Theta_k \right) \sin\left(\sum_{j=0}^{n} \Theta_j + \gamma \right) + \left(l_j \cos \sum_{k=0}^{j} \Theta_k \right) \cos\left(\sum_{j=0}^{n} \Theta_j + \gamma \right) \right) + \tau_n$$

which simplifies to

$$\tau_m = \frac{|\tau_n|}{c} \left(\sum_{j=m}^{n-1} \left(l_j \cos \sum_{k=j+1}^{n} \Theta_k \right) - \sum_{j=m}^{n-1} \left(l_j \sin \sum_{k=j+1}^{n} \Theta_k \right) \tan\gamma \right) + \tau_n$$

Monotonicity in γ

To show the monotonicity of the torques in the direction γ of the force, τ_m has to be differentiated with respect to γ resulting in

$$\frac{\partial \tau_m}{\partial \gamma} = -\frac{|\tau_n|}{c} \sum_{j=m}^{n-1} \left(l_j \sin \sum_{k=j+1}^{n} \Theta_k \right) \frac{1}{\cos^2\gamma}$$

which is continuous for $\gamma \neq (2k+1)\frac{\pi}{2} \;:\; k \in Z$ and has no local maxima or minima. The torque τ_m is therefore monotonic in γ for $\gamma \in \left((2k-1)\frac{\pi}{2}, (2k+1)\frac{\pi}{2} \right)$.

Monotonicity in c

In a similar way, the monotonicity in c can be shown by the following derivative

$$\frac{\partial \tau_m}{\partial c} = -\left|\tau_n\right| \left(\sum_{j=m}^{n-1} \left(l_j \cos \sum_{k=j+1}^{n} \Theta_k \right) - \sum_{j=m}^{n-1} \left(l_j \sin \sum_{k=j+1}^{n} \Theta_k \right) \tan\gamma \right) \frac{1}{c^2}$$

which is again continuous for $c \neq 0$ and without local extrema, meaning that τ_m is also monotonic in c for $c \in (-\infty, 0)$ or $c \in (0, \infty)$.

References

[1] P.K. Allen. Integrating vision and touch for object recognition tasks. *International Journal of Robotics Research*, 7(6):15–33, 1988.

[2] P. Dario and G. Buttazzo. An anthropomorphic robot finger for investigating artificial tactile perception. *International Journal of Robotics Research*, 6(3):25–48, 1987.

[3] R.E. Ellis. Planning tactile recognition paths in two and three dimensions. *International Journal of Robotics Research*, 11(2):87–111, 1992.

[4] A. Gelb, editor. *Applied Optimal Estimation.* M.I.T. Press, Cambridge, MA, 1974.

[5] S.J. Gordon and W.T. Townsend. Integration of tactile-force and joint-torque information in a whole-arm manipulator. In *Proceedings of the IEEE International Conference on Robotics and Automation*, pages 464–469, Scottsdale, AZ, May 1989. IEEE.

[6] R.A. Grupen. Planning grasp strategies for multifingered robot hands. In *Proceedings of the IEEE International Conference on Robotics and Automation*, pages 646–651, Sacramento, CA, April 1991. IEEE.

[7] R.A. Grupen, T.C. Henderson, and I.D. McCammon. A survey of general purpose manipulation. *International Journal of Robotics Research*, 8(1):38–62, 1989.

[8] R.A. Grupen and R.S. Weiss. Force domain models for multifingered grasp control. In *Proceedings of the IEEE International Conference on Robotics and Automation*, pages 418–423, Sacramento, CA, April 1991. IEEE.

[9] M. Kaneko, H. Maekawa, and K. Tanie. Active tactile sensing by robotic fingers based on minimum-external-sensor-realization. In *Proceedings of the IEEE International Conference on Robotics and Automation*, pages 1289–1294, Nice, France, May 1992. IEEE.

[10] M. Kaneko and K. Tanie. Contact point detection for grasping of an unknown object using self-posture changeability (spc). In *Proceedings of the IEEE International Conference on Robotics and Automation*, pages 864–869, Cincinnati, OH, May 1990. IEEE.

[11] H.R. Nicholls and M.H. Lee. A survey of robot tactile sensing technology. *International Journal of Robotics Research*, 8(3):3–30, 1989.

[12] J.R. Phillips, R.S. Johansson, and K.O. Johnson. Responses of human mechanoreceptive afferents to embossed dot arrays scanned across fingerpad skin. *Journal of Neuroscience*, 12(3):827–839, 1992.

[13] F. Reuleaux. *The Kinematics of Machinery.* reprinted by Dover Publications, INC., New York, NY, 1963. Translated and Edited by A.B.W. Kennedy in 1876.

[14] S.A. Stansfield. A haptic system for a multifingered hand. In *Proceedings of the IEEE International Conference on Robotics and Automation*, pages 658–664, Sacramento, CA, April 1991. IEEE.

[15] D.A. Sugden. Role of proprioception in eye-hand coordination. In *Development of Eye-Hand Coordination Across the Life Span*, pages 133–153. University of South Carolina Press, 1990.

[16] T. Tsujimura and T. Yabuta. A tactile sensing method employing force/torque information through insensitive probes. In *Proceedings of the IEEE International Conference on Robotics and Automation*, pages 1315–1320, Nice, France, May 1992. IEEE.